A novel high-content phenotypic screen to identify inhibitors of mitochondrial DNA maintenance in trypanosomes

A novel high-content phenotypic screen to identify inhibitors of mitochondrial DNA maintenance in trypanosomes

Running title: Screening for trypanosome mtDNA maintenance inhibitors

Migla Miskinyte[a], John C. Dawson[b], Ashraff Makda[b], Dahlia Doughty-Shenton[c], Neil O. Carragher[b], and Achim Schnaufer[a#]

[a]Institute of Immunology & Infection Research, University of Edinburgh, Edinburgh, United Kingdom

[b]Cancer Research UK Edinburgh Centre, MRC Institute of Genetics and Molecular Medicine, University of Edinburgh, United Kingdom

[c]MRC Centre for Reproductive Health, The Queen's Medical Research Institute, University of Edinburgh, United Kingdom

#Address correspondence to Achim Schnaufer, achim.schnaufer@ed.ac.uk

Abstract

Kinetoplastid parasites cause diverse neglected diseases in humans and livestock, with an urgent need for new treatments. Survival of kinetoplastids depends on their uniquely structured mitochondrial genome (kDNA), the eponymous kinetoplast. Here we report development of a high-content screen for pharmacologically induced kDNA loss, based on specific staining of parasites and automated image analysis. As proof-of-concept we screened a diverse set of ~14,000 small molecules and exemplify a validated hit as a novel kDNA-targeting compound.

Keywords: High-throughput screening, high-content screening, trypanosomatids, kinetoplast, kDNA, mitochondria

Introduction, methods, results and discussion combined

Kinetoplastids cause diverse, life-threatening diseases in humans and their livestock, namely African sleeping sickness (1), Chagas disease (2) and the leishmaniases (3) in the former and animal trypanosomiasis in the latter (4). These diseases particularly affect populations in low- and middle-income countries in many parts of the world. Currently available drugs are unsatisfactory because they cause severe, and sometimes lethal, side-effects, they are difficult to administer, and resistance continues to emerge, necessitating the development of novel anti-kinetoplastid therapies (5, 6).

Although kinetoplastids have evolved distinct methods of infection and host immune evasion, they all share a unique biological feature: the organisation of their mitochondrial DNA (mtDNA, or kDNA in these organisms) in a peculiar structure that gave these organisms their name: the kinetoplast (7). The kDNA is extremely complex, containing hundreds of different classes of 'guide RNA'-encoding minicircles of variable copy number which are essential for post-transcriptional RNA editing in these organisms (8–10). Together with dozens of maxicircles, which are the equivalent of mtDNA in other eukaryotes and encode subunits of the respiratory chain, F_1F_O-ATP synthase and mitoribosomes, thousands of minicircles form an interlinked network structure. The kDNA is thus intrinsically different from mammalian mtDNA, is essential for parasite survival (11, 12) and is a validated target for some current anti-

trypanosomatid therapies (13–16), making it an attractive target for discovery of new, improved drugs (17, 18).

Uniquely among kinetoplastids, the sole function of kDNA in bloodstream form *T. brucei* is the production of subunit *a* of the F_1F_O-ATPase (19), which in this stage of the parasite's life cycle operates in reverse to maintain the mitochondrial membrane potential (20). The respiratory chain and oxidative phosphorylation - classical mitochondrial functions - are not functional in bloodstream stage *T. brucei*. Facilitated by this limited function, kDNA-independent mutants have evolved in *T. brucei* subspecies that cause trypanosomiasis in animals (19, 21, 22). Typically, kDNA independence in *T. brucei* is caused by a mutation in the nuclearly encoded subunit γ of the mitochondrial F_1F_O-ATPase (19). Importantly, kDNA independence has never been reported for those kinetoplastid parasites of humans and livestock that are currently responsible for by far the greatest disease and economic burden, i.e. *Leishmania* spp., *T. cruzi*, *T. vivax* and *T. congolense*. This remains to be the case despite decades of use of ethidium bromide (EtBr) and isometamidium chloride (phenanthridine compounds that strongly affect kDNA) for the treatment of African animal trypanosomiasis (14–16, 23–25). Loss of kDNA can apparently not be compensated for in these species, either because additional kDNA-encoded genes are essential (clearly the case for *Leishmania* and *T. cruzi*, which depend on a functional respiratory chain throughout their life cycle (26)), or because the mutations in F_1F_O-ATPase γ that can compensate for loss of kDNA in bloodstream *T. brucei* are not functional in these species. Novel anti-trypanosomatid therapies based on inhibition of kDNA maintenance are therefore attractive (17, 18).

Drug discovery efforts are typically either phenotypic or target-based (27, 28). While target-based campaigns have dominated efforts for decades, they often fail to produce new

65 therapeutic molecules due to the challenge of translating promising results from reductionist
66 biochemical and cellular assays into robust efficacy in more complex *in vivo* models (29). In
67 contrast, phenotypic screens are often more time-consuming and expensive, and the mode(s) of
68 action behind any identified hits are usually unknown (29). However, both approaches are
69 complimentary and can be used synergistically to fast-track the identification of target-specific
70 compounds that can enter the cell and reach the associated intracellular organelles to induce the
71 desired effect. This paper describes the design, implementation and validation of a phenotypic
72 high-content screen (HCS) with automated image analysis for the discovery of hit compounds
73 that specifically target kDNA maintenance, using *Trypanosoma brucei brucei* (hereafter referred
74 to as *T. brucei*), a causative agent of animal trypanosomiasis, as a model system.

75 **HTS design and image analysis**. To enable the discovery of target-specific compounds,
76 our phenotypic screen uses a genetically engineered kDNA-independent bloodstream form *T.*
77 *brucei* cell line which tolerates kDNA loss due to an L262P mutation in the nuclearly encoded
78 subunit γ of the mitochondrial F_1F_O-ATPase (19). Non-specific cytocidal or cytostatic
79 compounds, or more general inhibitors of mitochondrial function, which would be more likely to
80 cause side effects in the host, can readily be identified in this genetic background.

81 Our HCS has been optimized for use in a high throughput 384-well format (V-bottom,
82 Greiner-Bio, #781280), using a Biomek FX liquid handler (Beckman) to dilute all compounds
83 and subsequently adding L262P *T. brucei* cells using a VIAFLO multi-well plate liquid handler
84 (Integra) in a class II biosafety cabinet. Briefly, 2.5 µl compound (at a concentration of 200 µM
85 in culture medium with 2% dimethyl sulfoxide (DMSO)) were added to each well. Subsequently,
86 47.5 µl of parasite culture in complete HMI-9 medium (30), supplemented with 20% (v/v) fetal
87 calf serum, were seeded at 50 cells per well, giving a total volume of 50 µl with 1 x 10^3 cells/ml

and a final compound concentration of 10 μM. Plates were incubated in an atmosphere of 5% CO_2 at 37°C for 4 days (31). Following incubation, cells were stained with the cytoplasmic viability stain, 5(6)-carboxyfluorescein diacetate succinimidyl ester (CFDA-SE; CAS: 150347-59-4) at 10 μM for 15 mins at 37°C and, consecutively and without any washing steps, with Hoechst 33342 nucleic acid stain at 1 μg/mL for 5 minutes at 37°C. Subsequently, cells were fixed with 2% (w/v; final concentration) formaldehyde, with vigorous mixing to avoid clumped cells, a step that is crucial for subsequent image analysis (Fig. 1A). After 24 h fixation at 4°C, cells were washed 3 times with phosphate-buffered saline by centrifuging plates at 1,000 x g for 1 min to remove any remaining dye. Loss of cells during washing steps was minimised by using V-bottom plates and carefully adjusting fixed pipette positions for the Biomek FX liquid handler. Cells were then transferred into 384-well F-bottom plates for imaging (Greiner-Bio, #781986). The plates were centrifuged at 1,000 x g for 5 min prior to imaging acquisition at 40x magnification using an automated ImageXpress-XLS micro (Molecular Devices) HCS system. Each well was imaged across four different fields of view using DAPI (for Hoechst 33342 stain) and FITC (for CFDA-SE) filter sets. Image analysis was performed using the CellProfiler 3.1.9 software (32). Briefly, nuclear DNA and kDNA were identified based on area size of Hoechst 33342 positive objects, and viable cells were identified using the FITC channel (Fig. 1B, Fig. S1).

HCS performance validation and pilot screen. Plates (n=2) were prepared as above, with even-numbered columns containing a negative control (0.1% DMSO) and odd-numbered columns containing 10 nM EtBr (in 0.1% (v/v) DMSO), a known inhibitor of kDNA maintenance, as a positive control (15). A 'robust' *Z'* assay performance score of 0.725 was calculated (33, 34), indicating excellent performance (35).

To test the ability of our HCS to identify novel inhibitors of kDNA maintenance, 13,486 compounds were screened, from a diverse set of chemical libraries: Prestwick Chemical Library (Prestwick Chemical; 1,280 compounds), Screen-Well PKE library (Enzo Biochem; consisting of protease (53), kinase (80) and epigenetic (43) inhibitors), and BioAscent 12K diverse chemical libraries (BioAscent Discovery Ltd; 11,970 compounds). The Prestwick Chemical library was designed to represent broad pharmacological diversity of all FDA-approved small molecule drug classes and consists of drugs with known pharmacology, toxicology and pharmacokinetic properties to support repurposing of existing drugs. The BioAscent 12K compound library is a subset representing the chemical diversity of a 125,000-compound parent library, enabling subsequent expansion of screening hits to explore structure-activity relationships. All compounds were screened at a final concentration of 10 μM in ‘0.1% (v/v) DMSO in a 384-well format, where the first four columns had alternating positive (EtBr) and negative (DMSO) controls. Additionally, the PKE and Prestwick Chemical libraries were also screened at a lower final concentration of 1 μM because both libraries have been reported to lead to the identification of potent inhibitors in different phenotypic screening assays at this lower dose which may better reflect on-target rather than off-target activity observed at higher doses (36, 37). The screens were performed in 5 batches (48 plates in total), with a ‘robust’ *Z’* assay performance score (34) ranging from 0.63 to 0.9 between batches. The HCS identified 152 compounds with a reduced ratio of kDNA per nucleus (*Z*-score < -2; Fig. 2 and Table S1). Separate results for nucleus and kDNA counts for all wells are shown in Fig. S2.

Hit validation. For the top 50 compounds, based on ranking by kDNA/nucleus ratio (excluding all compounds that had less than 50 DNA objects per well) and a *Z*-score < -2 (Table S1), we manually reviewed the microscopy images for evidence of complete kDNA loss. Ten

candidates (Table S1) were cherry-picked for follow-up analysis based on consistently observed loss of kDNA from cells treated with these compounds and on their commercial availability. Purchased compounds were dissolved in DMSO, and their potency against wild type (WT) *T. brucei* cells was evaluated using an adapted 3-day Alamar Blue method (19). Only two compounds, (S)-propranolol hydrochloride and 1-(1-Adamantyl)-4-[(2-methoxy-4,5-dimethylphenyl)sulfonyl]piperazine (AMDSP, BioAscent code BCC0052412) were sufficiently potent at the highest concentration that could be tested (due to limited solubility in water) to permit calculation of IC_{50} values for WT cells of 16-22 µM and 1.6-2.3 µM, respectively (95% confidence intervals, Table S1; the other 8 compounds did not significantly effect growth of WT cells in the Alamar Blue assay). Next, we assessed the specificity of these two compounds as inhibitor of kDNA maintenance. This specificity is indicated by the selectivity for killing of kDNA-dependent ('WT') and kDNA-independent ('L262P'), but otherwise isogenic *T. brucei* cells. The most specific compound reported to date is EtBr, with a selectivity index of ~300 in the modified Alamar Blue assay (38). One the two compounds tested, AMDSP (Fig. 3A), reproducibly affected the viability of WT *T. brucei* cells at a lower concentration compared to L262P cells (Fig. 3B). The IC_{50} for WT cells was 1.9 µM, while the IC_{50} for L262P cells was estimated to be in the range of 8 µM (the value could not be determined more precisely due to poor compound solubility in DMSO at higher than 12.5 mM stock concentration). To investigate the time required for AMDSP to affect growth, we performed growth curves in WT and L262P cells at a final compound concentration of 12.5 µM in 0.1% (v/v) DMSO (Fig. 3C and 3D). After 3 days of AMDSP treatment, growth of WT cells was much more severely inhibited compared to L262P cells. No growth was observed between days 3 and 4 for one of the WT replicates (Fig. 3C, open red circles). The cumulative growth curve for the other replicate indicated a slight

increase in cell numbers between days 3 and 4 (Fig. 3C, filled red circles). However, by microscopy, we found no intact and motile WT cells after 4 days for either WT replicate, even after concentration of the culture by centrifugation, while L262P cells survived. Hence, it is more likely that the apparent increase for one of the WT replicates was caused by counting of cell debris in the Coulter machine. Moreover, we observed a substantial increase in the proportion of cells with complete loss of kDNA (0K1N cells) in WT and L262P cells after 2 or 3 days of exposure to 12.5 µM AMDSP (Fig. 4A). Interestingly, loss of kDNA was more severe for WT cells than for L262P cells. This could suggest a reduced uptake of AMDSP in L262P cells, perhaps caused by the lower mitochondrial membrane potential in these cells (39). In further support of an effect of AMDSP on kDNA maintenance, for the proportion of WT cells that had retained at least some kDNA after AMDSP-treatment, we observed a significant kDNA reduction in size compared to control cells (Fig. 4B), while the size of the nucleus was not affected (Fig. S3).

Altogether, these data confirm that an important part of the mode of action of AMDSP in trypanosomes is interference with kDNA maintenance. The data are consistent with the dynamics of growth inhibition and effects on kDNA of other compounds that preferentially target this structure, such as EtBr (39–41), although, unsurprisingly, potency and selectivity of this primary hit are much lower. Nonetheless, AMDSP may represent a promising starting point for hit-to-lead development. The compound is composed of piperazine, benzene and adamantane rings with a tertiary sulfonamide group. Adamantane derivatives, such as the well-studied drug, amantadine (1-amino-adamantane), show good pharmacokinetics in humans, are licensed drugs for the treatment of Parkinson's disease, and in the past had been used for the treatment of influenza, until emergence of resistance halted its application for this purpose (42). Moreover,

the discovery of amino-adamantane derivatives with trypanocidal activity (43) has spurred efforts for the recent development of more potent adamantane-benzene derivatives (44). Piperazine-based anti-helminthic drugs (45) have also gained interest in drug design studies because of their trypanocidal activity (46). The exact mechanism(s) by which the described derivatives affect trypanosomatids remains unknown but, based on our findings, effects on kDNA should be explored. Furthermore, similarity searches with AMDSP of the full BioAscent library suggest up to 150 related compounds that could be tested against trypanosomatids in the future to explore structure-activity relationships.

Identification of other anti-trypanosomatid compounds with unknown mode of action. In addition to a novel inhibitor of kDNA maintenance, we also identified compounds that strongly affected the viability of the kDNA-independent *T. brucei* cell line used for screening and that therefore must act via a different mechanism. To find such trypanocidal or trypanostatic hits, we first corrected for positional growth effects in our plates using the median polish normalisation method (47, 48) (Fig. S4). Median polish normalisation was performed in Spotfire software (PerkinElmer) using the High Content Profiler package to remove row and column biases. This method uses the row and column medians to identify the row and column effect on the data. We then scored for hits affecting *T. brucei* viability based on less than 10 total nuclei per image with *Z*-scores < -1. We identified 337 hits, corresponding to a hit rate of 2.5% (Table S2; Fig. S5, left panel). These include 31 compounds from the Prestwick Chemical Library that inhibited trypanosome growth at both 10 μM and 1 μM (double underline in Table S2), suggesting a good starting potency for any lead development efforts. Incidentally, among the compounds tested in our proof-of-concept screen were 9 compounds with known anti-trypanosomatid activity (49). Seven of these compounds were among the hits with a *Z*-score < -1

(highlighted in Table S2, right panel in Fig. S5). This further confirms the robustness of our HCS assay and suggests that, as an additional benefit, the outputs from this assay could also be used for the identification of anti-trypanosomatid compounds with a mode-of-action unrelated to kDNA maintenance.

In conclusion, we successfully established and validated a scalable, kDNA maintenance based phenotypic HCS with automated image analysis, using an engineered kDNA-independent *T. brucei* cell line as a kinetoplastid model system. A proof-of-concept screen of diverse small compound libraries identified and validated a novel compound affecting kDNA maintenance in *T. brucei*. To the best of our knowledge, this is the first HCS specifically designed to identify inhibitors of kDNA maintenance. Furthermore, we identified other anti-trypanosomatid compounds with activity in the low micromolar range (but with unknown molecular targets) that could be useful starting points for trypanosomatid drug development. In the future, the screen could be further optimised by trying to address the positional growth effects in plates and by developing machine learning algorithms that can lower the rate of false-positive hits and detect more subtle changes in kDNA, nuclear DNA and cell morphology.

Acknowledgements

M.M., J.D., D.D-S., N.O.C., A.M., and A.S. designed the research; M.M., J.D., A.S. analysed the data; M.M. performed the research; M.M. and A.S. wrote the paper.

We thank Zandile Nare for helpful discussions and Angus Morrison (BioAscent) for suggestions on BCC0052412 analogs.

This work was supported by Senior Non-Clinical Fellowship MR/L019701/1 from the UK Medical Research Council to A.S and Institutional Strategic Support Fund (ISSF3) award (reference IS3-R2.28) to A.S. for salary to M.M. and consumables.

References

1. Büscher P, Cecchi G, Jamonneau V, Priotto G. 2017. Human African trypanosomiasis. Lancet 390:2397–2409.

2. Álvarez-Hernández DA, Franyuti-Kelly GA, Díaz-López-Silva R, González-Chávez AM, González-Hermosillo-Cornejo D, Vázquez-López R. 2018. Chagas disease: Current perspectives on a forgotten disease. Rev Médica del Hosp Gen México 81:154–164.

3. Alves F, Bilbe G, Blesson S, Goyal V, Monnerat S, Mowbray C, Muthoni Ouattara G, Pécoul B, Rijal S, Rode J, Solomos A, Strub-Wourgaft N, Wasunna M, Wells S, Zijlstra EE, Arana B, Alvar J. 2018. Recent Development of Visceral Leishmaniasis Treatments: Successes, Pitfalls, and Perspectives. Clin Microbiol Rev 31:1–30.

4. Morrison LJ, Vezza L, Rowan T, Hope JC. 2016. Animal African Trypanosomiasis: Time to Increase Focus on Clinically Relevant Parasite and Host Species. Trends Parasitol In Press Corrected Proof.

5. Field MC, Horn D, Fairlamb AH, Ferguson MAJ, Gray DW, Read KD, De Rycker M, Torrie LS, Wyatt PG, Wyllie S, Gilbert IH. 2017. Anti-trypanosomatid drug discovery: An ongoing challenge and a continuing need. Nat Rev Microbiol 15:217–231.

6. De Rycker M, Baragaña B, Duce SL, Gilbert IH. 2018. Challenges and recent progress in drug discovery for tropical diseases. Nature 559:498–506.

7. Stuart K, Brun R, Croft S, Fairlamb A, Gürtler RE, McKerrow J, Reed S, Tarleton R. 2008. Kinetoplastids: Related protozoan pathogens, different diseases. J Clin Invest

118:1301–1310.

8. Cooper S, Wadsworth ES, Ochsenreiter T, Ivens A, Savill NJ, Schnaufer A. 2019. Assembly and annotation of the mitochondrial minicircle genome of a differentiation-competent strain of Trypanosoma brucei. Nucleic Acids Res 47:11304–11325.

9. Jensen RE, Englund PT. 2012. Network News: The Replication of Kinetoplast DNA. Annu Rev Microbiol 66:473–491.

10. Read LK, Lukeš J, Hashimi H. 2016. Trypanosome RNA editing: the complexity of getting U in and taking U out. Wiley Interdiscip Rev RNA 7:33–51.

11. Jensen RE, Englund PT. 2012. Network News: The Replication of Kinetoplast DNA. Annu Rev Microbiol 66:473–491.

12. Schneider A, Ochsenreiter T. 2018. Failure is not an option - mitochondrial genome segregation in trypanosomes. J Cell Sci 131.

13. Girard RMBM, Crispim M, Stolić I, Damasceno FS, Da Silva MS, Pral EMF, Elias MC, Bajić M, Silber AM. 2016. An aromatic diamidine that targets kinetoplast DNA, impairs the cell cycle in trypanosoma cruzi, and diminishes trypomastigote release from infected mammalian host cells. Antimicrob Agents Chemother 60:5867–5877.

14. Chowdhury AR, Bakshi R, Wang J, Yildirir G, Liu B, Pappas-Brown V, Tolun G, Griffith JD, Shapiro T a., Jensen RE, Englund PT. 2010. The killing of African trypanosomes by ethidium bromide. PLoS Pathog 6.

15. Gould MK, Schnaufer A. 2014. Independence from Kinetoplast DNA Maintenance and Expression Is Associated with Multidrug Resistance in Trypanosoma brucei In Vitro.

Antimicrob Agents Chemother 58:2925–8.

16. Yang G, Choi G, No JH. 2016. Antileishmanial mechanism of diamidines involves targeting kinetoplasts. Antimicrob Agents Chemother 60:6828–6836.

17. Sela D, Milman N, Kapeller I, Zick A, Bezalel R, Yaffe N, Shlomai J. 2008. Unique Characteristics of the Kinetoplast DNA Replication Machinery Provide Potential Drug Targets in Trypanosomatids BT - Drug Targets in Kinetoplastid Parasites, p. 9–21. *In* Majumder, HK (ed.), . Springer New York, New York, NY.

18. Chakraborty AK, Majumder HK. 1999. Molecular biology of Leishmania: Kinetoplast DNA and DNA topoisomerases as novel therapeutic targets. Curr Sci 76:1462–1472.

19. Dean S, Gould MK, Dewar CE, Schnaufer AC. 2013. Single point mutations in ATP synthase compensate for mitochondrial genome loss in trypanosomes. Proc Natl Acad Sci U S A 110:14741–14746.

20. Schnaufer A, Clark-Walker GD, Steinberg AG, Stuart K. 2005. The F1-ATP synthase complex in bloodstream stage trypanosomes has an unusual and essential function. EMBO J 24:4029–4040.

21. Carnes J, Anupama A, Balmer O, Jackson A, Lewis M, Brown R, Cestari I, Desquesnes M, Gendrin C, Hertz-Fowler C, Imamura H, Ivens A, Kořený L, Lai D-H, MacLeod A, McDermott SM, Merritt C, Monnerat S, Moon W, Myler P, Phan I, Ramasamy G, Sivam D, Lun Z-R, Lukeš J, Stuart K, Schnaufer A. 2015. Genome and Phylogenetic Analyses of Trypanosoma evansi Reveal Extensive Similarity to T. brucei and Multiple Independent Origins for Dyskinetoplasty. PLoS Negl Trop Dis 9:e3404.

22. Jensen RE, Simpson L, Englund PT. 2008. What happens when Trypanosoma brucei

leaves Africa. Trends Parasitol 24:428–431.

23. Thomas JA, Baker N, Hutchinson S, Dominicus C, Trenaman A, Glover L, Alsford S, Horn D. 2018. Insights into antitrypanosomal drug mode-of-action from cytology-based profiling. PLoS Negl Trop Dis 12:e0006980.

24. Walker R, Saha L, Hill GC, Chaudhuri M. 2005. The effect of over-expression of the alternative oxidase in the procyclic forms of Trypanosoma brucei. Mol Biochem Parasitol 139:153–162.

25. Giordani F, Morrison LJ, Rowan TG, De Koning HP, Barrett MP. 2016. The animal trypanosomiases and their chemotherapy: A review. Parasitology 143:1862–1889.

26. Michels PAM, Villafraz O, Pineda E, Alencar MB, Cáceres AJ, Silber AM, Bringaud F. 2021. Carbohydrate metabolism in trypanosomatids: New insights revealing novel complexity, diversity and species-unique features. Exp Parasitol 224:108102.

27. Gilbert IH. 2013. Drug Discovery for Neglected Diseases: Molecular Target- Based and Phenotypic Approaches. J Medic Chem.

28. Torrie LS, Zuccotto F, Robinson DA, Gray DW, Gilbert IH, De Rycker M. 2019. Identification of inhibitors of an unconventional Trypanosoma brucei kinetochore kinase. PLoS One 14:1–16.

29. Moffat JG, Vincent F, Lee JA, Eder J, Prunotto M. 2017. Opportunities and challenges in phenotypic drug discovery: An industry perspective. Nat Rev Drug Discov 16:531–543.

30. Hirumi H, Hirumi K. 1989. Continuous Cultivation of Trypanosoma brucei Blood Stream Forms in a Medium Containing a Low Concentration of Serum Protein without Feeder

311 Cell Layers Author (s): Hiroyuki Hirumi and Kazuko Hirumi Published by : Allen Press
312 on behalf of The American Soc. J Parasitol 75:985–989.

313 31. Schaffner-Barbero C, Miskinyte M, Grewal JS, Schnaufer A. 2018. Pharmacological
314 inhibition of the vacuolar atpase in bloodstream-form trypanosoma brucei rescues genetic
315 knockdown of mitochondrial gene expression. Antimicrob Agents Chemother 62:1–7.

316 32. Mcquin C, Goodman A, Chernyshev V, Kamentsky L, Cimini A, Karhohs KW, Doan M,
317 Ding L, Rafelski SM, Thirstrup D, Wiegraebe W, Singh S, Becker T, Caicedo JC,
318 Carpenter AE. 2018. CellProfiler 3.0: Next-generation image processing for biology.
319 PLoS Biol 16:1–17.

320 33. Zhang J-H, Chung TDY, Oldenburg KR. 1999. A Simple Statistical Parameter for Use in
321 Evaluation and Validation of High Throughput Screening Assays. J Biomol Screen 4:67–
322 73.

323 34. Atmaramani R, Pancrazio JJ, Black BJ. 2020. Adaptation of robust Z' factor for assay
324 quality assessment in microelectrode array based screening using adult dorsal root
325 ganglion neurons. J Neurosci Methods 339:108699.

326 35. Sittampalam G, Coussens N, Arkin M, Auld D, Austin C, Bejcek B, Glicksman M, Inglese
327 J, Iversen P, Mcgee J, Mcmanus O, Minor L, Napper A, Peltier JM, Riss T, Trask O,
328 Weidner J. 2016. Assay Guidance Manual. Assay Guid Man 305–336.

329 36. Marwick JA, Elliott RJR, Longden J, Makda A, Hirani N, Dhaliwal K, Dawson JC,
330 Carragher NO. 2021. Application of a High-Content Screening Assay Utilizing Primary
331 Human Lung Fibroblasts to Identify Antifibrotic Drugs for Rapid Repurposing in
332 COVID-19 Patients. SLAS Discov Adv life Sci R D 26:1091–1106.

37. Warchal SJ, Dawson JC, Shepherd E, Munro AF, Hughes RE, Makda A, Carragher NO. 2020. High content phenotypic screening identifies serotonin receptor modulators with selective activity upon breast cancer cell cycle and cytokine signaling pathways. Bioorg Med Chem 28:115209.

38. Gould MK, Schnaufer A. 2014. Independence from kinetoplast DNA maintenance and expression is associated with multidrug resistance in trypanosoma brucei in vitro. Antimicrob Agents Chemother 58:2925–2928.

39. Eze AA, Gould MK, Munday JC, Tagoe DNA, Stelmanis V, Schnaufer A, De Koning HP. 2016. Reduced Mitochondrial Membrane Potential Is a Late Adaptation of Trypanosoma brucei brucei to Isometamidium Preceded by Mutations in the γ Subunit of the F1Fo-ATPase. PLoS Negl Trop Dis 10:e0004791.

40. Dewar CE, MacGregor P, Cooper S, Gould MK, Matthews KR, Savill NJ, Schnaufer A. 2018. Mitochondrial DNA is critical for longevity and metabolism of transmission stage Trypanosoma brucei. PLOS Pathog 14:e1007195.

41. Chowdhury AR, Bakshi R, Wang J, Yildirir G, Liu B, Pappas-Brown V, Tolun G, Griffith JD, Shapiro TA, Jensen RE, Englund PT. 2010. The killing of African trypanosomes by ethidium bromide. PLoS Pathog 6.

42. Chang C, Ramphul K. 2021. Amantadine. Treasure Island (FL).

43. Kelly JM, Quack G, Miles MM. 2001. In vitro and in vivo activities of aminoadamantane and aminoalkylcyclohexane derivatives against Trypanosoma brucei. Antimicrob Agents Chemother 45:1360–1366.

44. Georgiadis M-O, Kourbeli V, Papanastasiou IP, Tsotinis A, Taylor MC, Kelly JM. 2020.

355 Synthesis and evaluation of novel 2,4-disubstituted arylthiazoles against T. brucei . RSC
356 Med Chem 11:72–84.

357 45. Lappin MR. 2013. Chapter 37 - Anthelmintic Agents, p. 458–462. *In* Washabau, RJ, Day,
358 MJBT-C and FG (eds.), Canine and Feline Gastroenterology. W.B. Saunders, Saint Louis.

359 46. Huang TL, Bacchi CJ, Kode NR, Zhang Q, Wang G, Yartlet N, Rattendi D, Londono I,
360 Mazumder L, Vanden Eynde JJ, Mayence A, Donkor IO. 2007. Trypanocidal activity of
361 piperazine-linked bisbenzamidines and bisbenzamidoxime, an orally active prodrug. Int J
362 Antimicrob Agents 30:555–561.

363 47. Brideau C, Gunter B, Pikounis B, Liaw A. 2003. Improved statistical methods for hit
364 selection in high-throughput screening. J Biomol Screen 8:634–647.

365 48. Tukey JW. 1977. Exploratory data analysis. Addison-Wesley Pub. Co., Reading, Mass.

366 49. MacKey ZB, Baca AM, Mallari JP, Apsel B, Shelat A, Hansell EJ, Chiang PK, Wolff B,
367 Guy KR, Williams J, McKerrow JH. 2006. Discovery of trypanocidal compounds by
368 whole cell HTS of Trypanosoma brucei. Chem Biol Drug Des 67:355–363.

369

370 **Figure legends**

371

372 **FIG 1**. **High-content screening (HCS) strategy to identify compounds inhibiting kDNA**
373 **maintenance in *T. brucei.* (A)** Representative fluorescence microscopy images of *T. brucei*
374 using the HCS staining protocol. From left to right: Hoechst 33342 staining of trypanosome
375 nuclei and kDNA (in magenta), CFDA-SE cytoplasmic viability stain (in green), phase contrast,

and merged images. **(B)** Schematic representation of the image analysis pipeline using CellProfiler. First, nuclei and kDNA were identified from the Hoechst 33342 staining (upper left panel). Next, nuclei and kDNA were separated by classifying stained objects according to area size (upper right and lower right panels; nuclei ≥ 60 area size in arbitrary units, green in lower right panel; kDNA < 60 area size, magenta in lower right panel; bin width = 20 with bin centre ranging from 0 to 200). Finally, viable cells were identified using the CFDA-SE cytoplasmic viability stain (lower left panel). Each well was imaged at four different, non-overlapping positions.

FIG 2. **HCS result and hit selection.** Tested compounds were ranked based on the decrease of kDNA/nucleus ratio in imaged wells (*Z*-score < -2 (dashed black line)), resulting in 152 hits (see also Table S1). Images of the top 50 hits (based on ranking by decrease in kDNA/nucleus ratio) were then re-examined using ImageJ software. Ten compounds were selected for follow-up analysis, based on complete loss of kDNA observed and on commercial availability (highlighted by the black triangles).

FIG 3. **Hit validation. (A)** Structure of AMDSP (BCC0052412). **(B)** Dose-response curves for the effect of AMDSP on growth of kDNA-dependent (WT, black squares) and kDNA-independent (L262P, red squares) bloodstream form *T. brucei*. **(C)** Cumulative growth curves of bloodstream form *T. brucei* cells cultured in the presence (dashed lines) and absence (solid lines, filled circles) of 12.5 µM AMDSP (red) or 10 nM EtBr (blue). Growth curves in the presence of solvent only are shown as controls (0.1% DMSO, black). Cell numbers were determined with a

Coulter counter. **(D)** Comparison of cumulative cell numbers in **(C)** after 96 h between WT and L262P cells. Student unpaired t-test, $p < 0.00005$ (****). All experiments were performed in triplicate; in addition, the effect of AMDSP on WT and L262P cells was tested on two separate occasions (Test 1 and Test 2).

FIG 4. **AMDSP effects kDNA maintenance. (A)** Loss of kDNA (0K1N cells = cells with no kinetoplast and one nucleus) assessed by DAPI staining and microscopy after 2 days (D2) and 3 days (D3) of culturing in the presence or absence of 12.5 µM AMDSP. Statistical significance of differences was assessed with the Student unpaired t-test; $P \leq 0.05$ (*), $P \leq 0.01$ (**), $P \leq 0.001$ (***). **(B)** The relative amount of kDNA in 1K1N cells (cells with 1 kinetoplast and 1 nucleus) after 2 days of culturing was assessed by DAPI staining and quantitation of kinetoplast versus nucleus fluorescence intensity. Statistical significance of differences was assessed with the Mann-Whitney test; $P < 0.001$ (***) for AMDSP at 12.5 µM in 0.1% DMSO (n = 90) versus 0.1% DMSO (n = 90); $P < 0.001$ (***). All experiments were performed in triplicate.

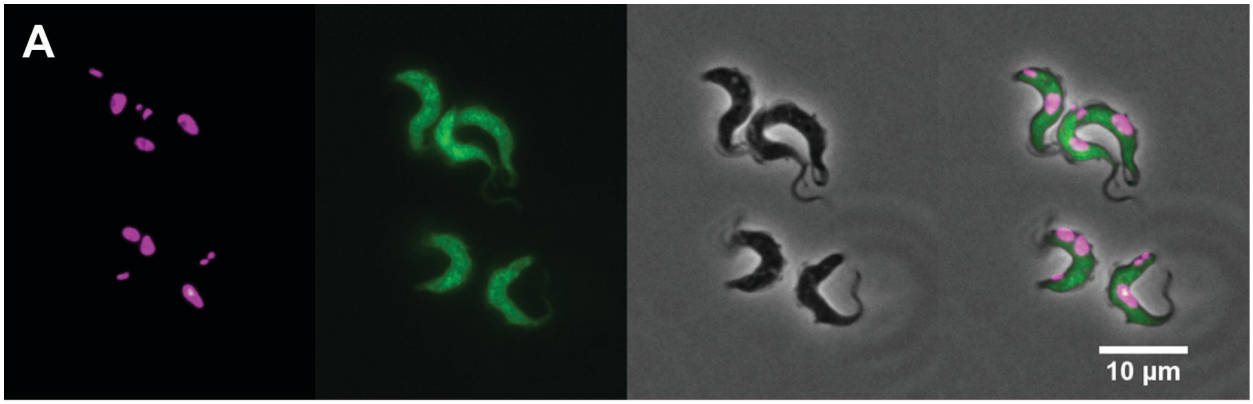

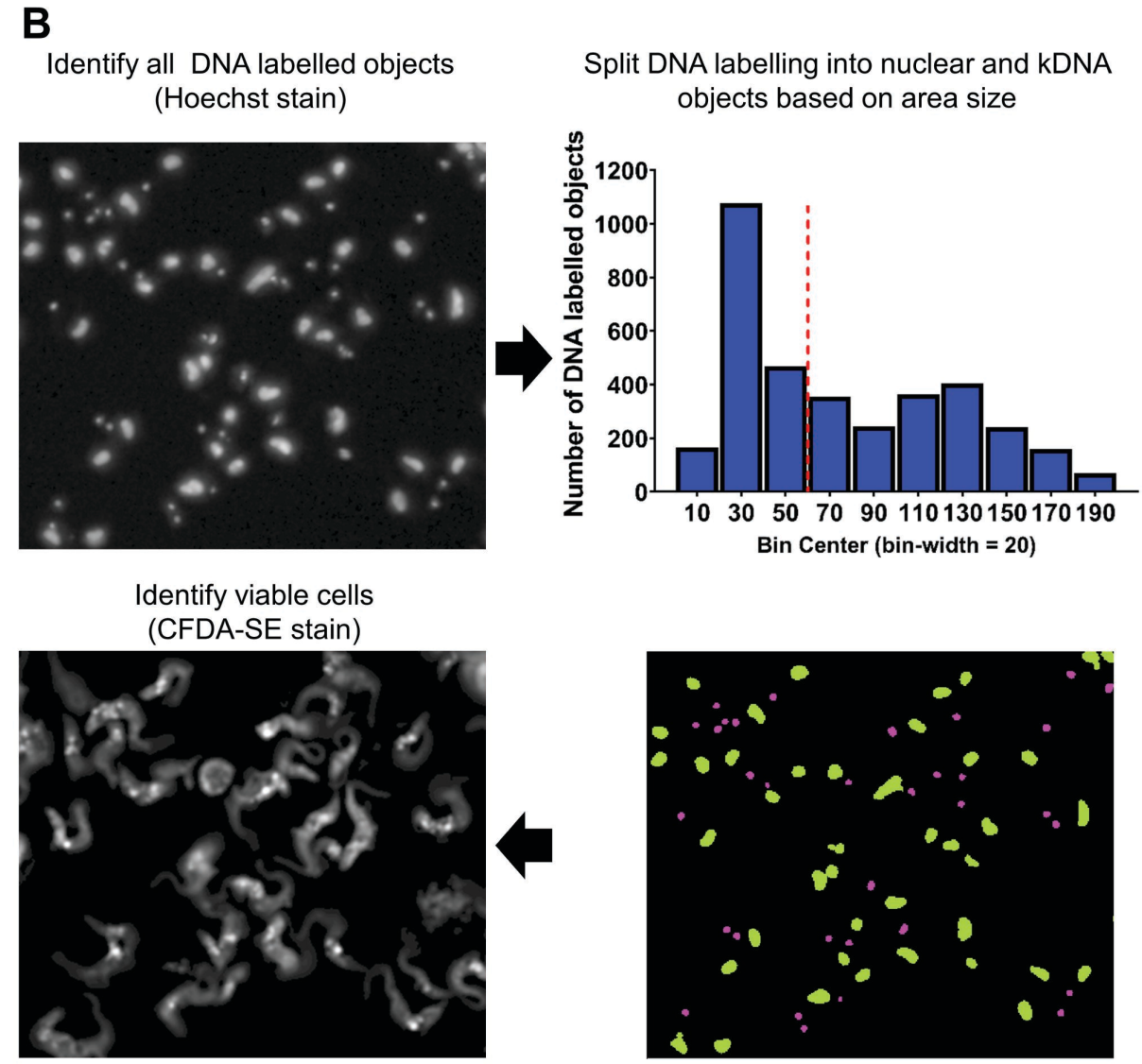

FIG 1

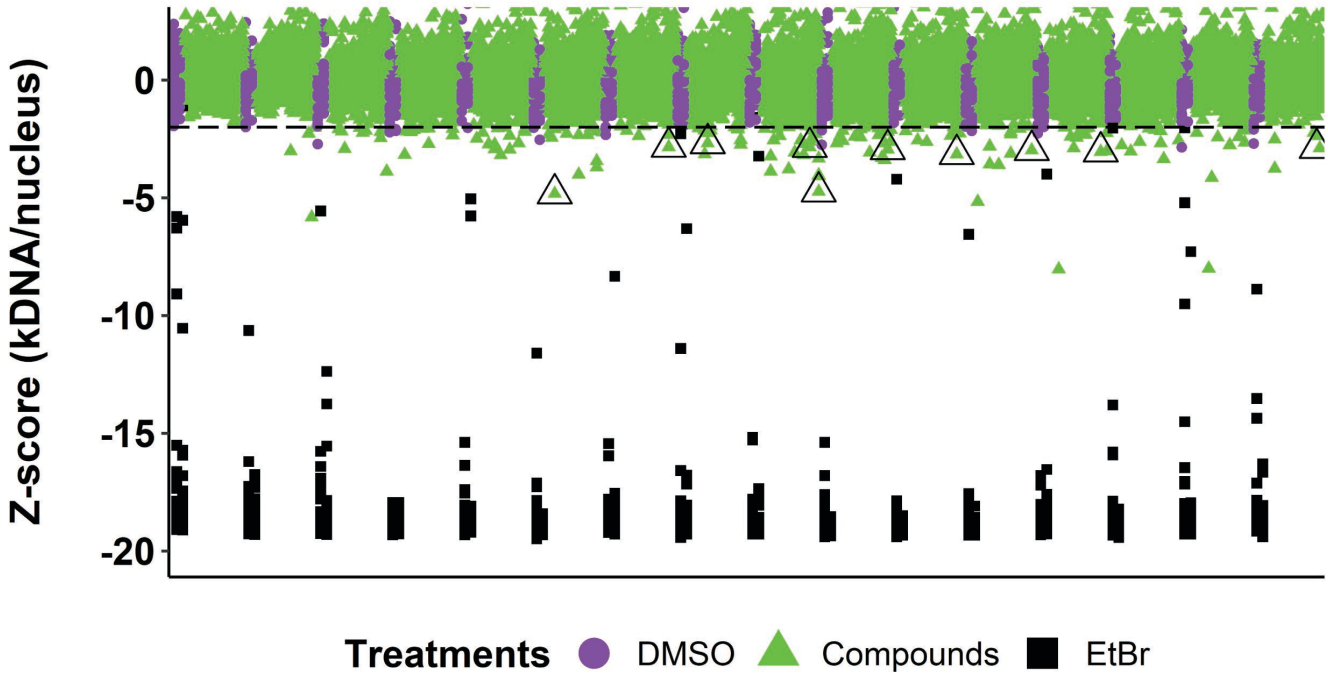

FIG 2

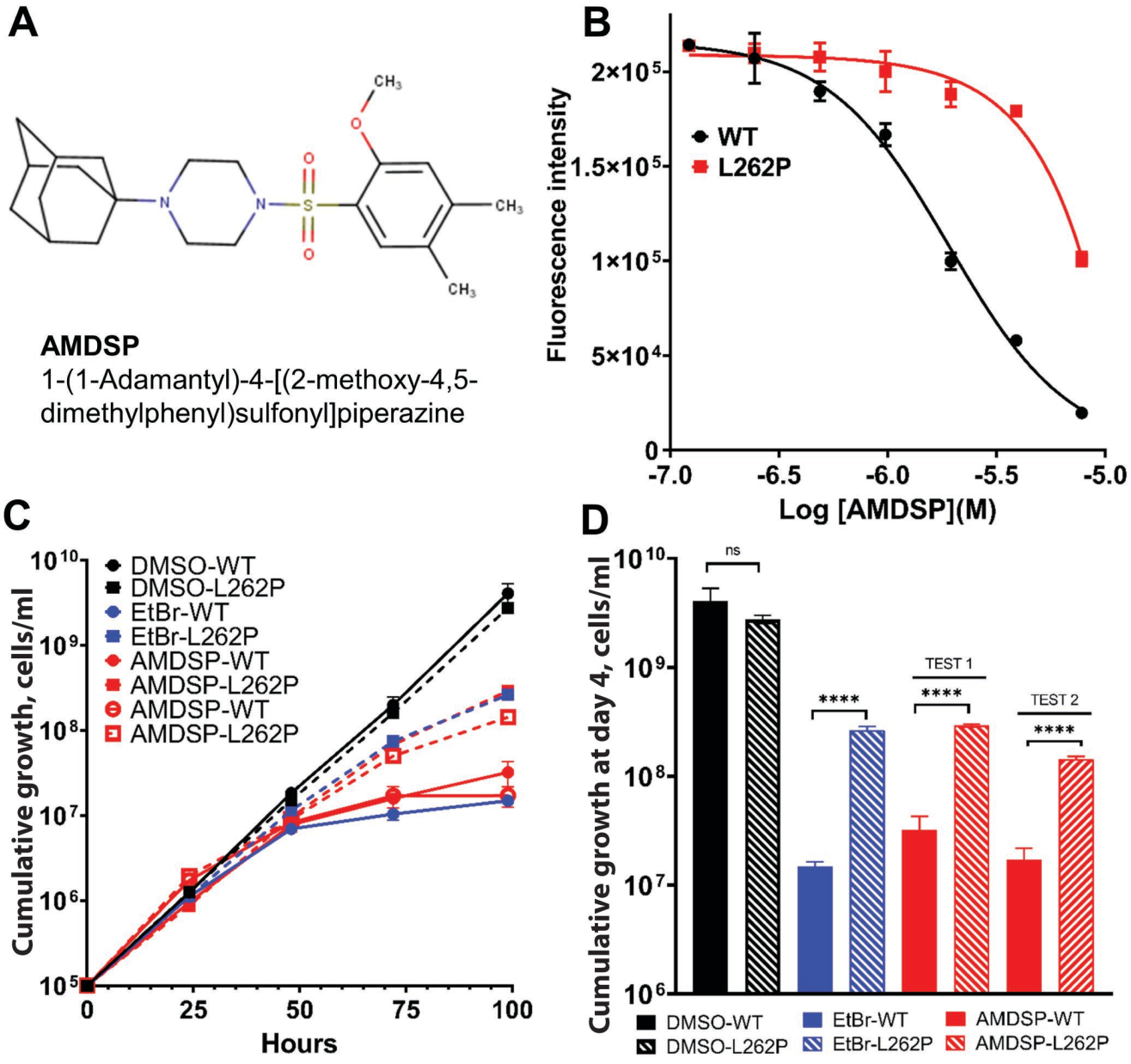

FIG 3

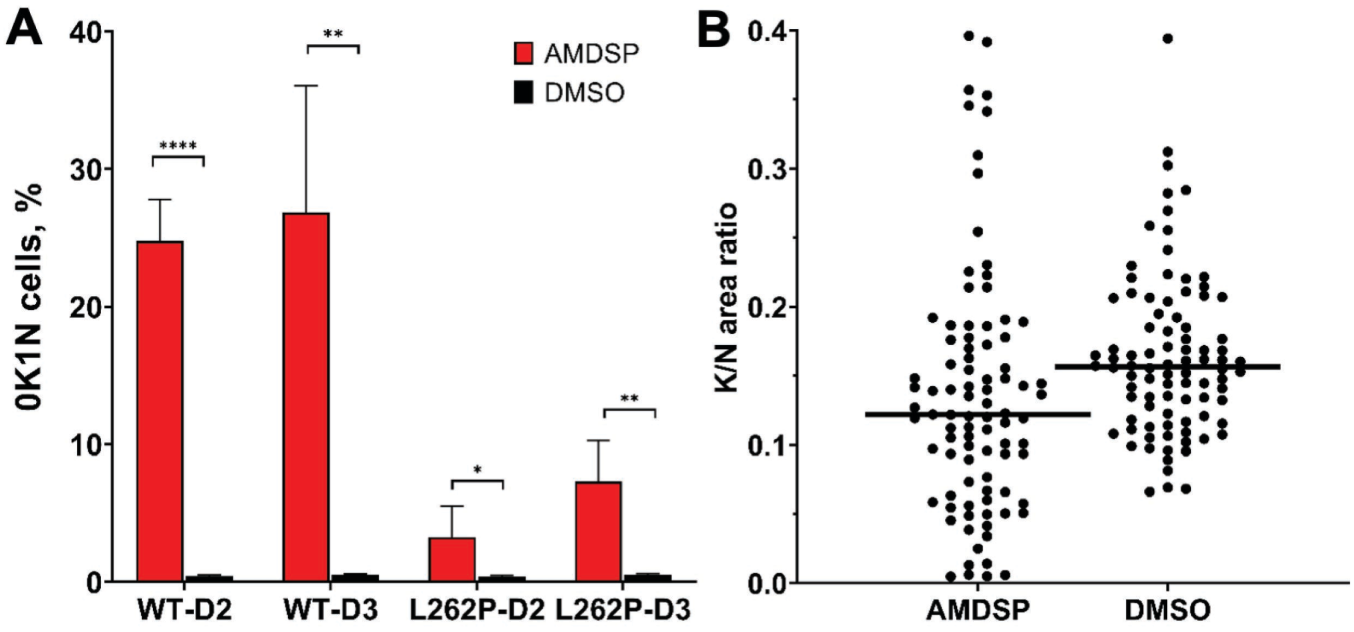

FIG 4